Mound slope and shape selection during unstable multilayer growth: Analysis of step-dynamics models including downward funneling

Maozhi Li[1] and J. W. Evans[2]

[1]*Institute of Physical Research and Technology, and Ames Laboratory−USDOE, Iowa State University, Ames, Iowa 50011, USA*
[2]*Department of Mathematics, and Ames Laboratory−USDOE, Iowa State University, Ames Iowa 50011, USA*
(Received 16 November 2005; published 28 March 2006)

Step-dynamics models are developed for mound shape evolution during multilayer homoepitaxial growth in the presence of inhibited interlayer transport. Unconventionally, our models also incorporate downward funneling (DF) of atoms deposited at step edges. The extent of DF can be reduced continuously to zero where one recovers traditional step dynamics models. This allows direct comparison between the behavior of models with and without DF. We show that DF greatly enhances growth of the height of valleys at the mound bases to an extent compatible with slope selection. To elucidate the selected shapes of finite mounds, we consider a suitably defined net flux of adatom attachment at steps summed over a mound side between valley and peak. This quantity varies periodically but vanishes when further averaged over time, a condition which directly constrains the selected mound shapes. We also characterize the dependence of these shapes on the prescription of nucleation of new islands at the mound peak.

I. INTRODUCTION

The morphological evolution of thin films during epitaxial growth is a topic of fundamental and technological interest. Even for homoepitaxial growth, the interplay between deposition of atoms and various inhibited surface diffusion processes gives rise to a rich variety of far-from-equilibrium surface morphologies.[1,2] In homoepitaxy, atoms are deposited onto and diffuse across the surface, and then aggregate into two-dimensional (2D) islands. For atoms subsequently deposited on top of islands, there typically exists an additional Ehrlich-Schwoebel (ES) step edge barrier inhibiting interlayer transport.[3,4] The presence of such an ES barrier leads to unstable film growth characterized by kinetic roughening and the formation of three-dimensional (3D) mounds, i.e., multilayer stacks of 2D islands.

This unstable growth mode was explained by Villain as follows.[5,6] The presence of an ES barrier implies that diffusing atoms tend to be reflected from descending steps and incorporated into ascending steps. This diffusion bias produces a destabilizing lateral mass current in the uphill direction. A number of homoepitaxial growth experiments have revealed not only mounded morphologies, but also suggested the development of a well-defined selected mound slope following a regime of steepening of mound sides.[7–11] The latter feature has been associated with the presence of nonthermal dynamical processes related to the downward transport of atoms deposited near step edges.[12–15] One example of such a process is "downward funneling" (DF).[16–18] Molecular dynamics simulations reveal that atoms deposited at step edges or on the sides of multilayer nanoprotrusions in metal(100) systems[16,19–21] or metal(111) systems[22] funnel down to fourfold-hollow or threefold-hollow adsorption sites, respectively, in lower layers. Unstable growth behavior has been explored utilizing kinetic Monte Carlo simulation of both generic and realistic atomistic lattice-gas models with considerable emphasis on the slow coarsening of mound dimensions following slope selection.[11,14,15,23,24]

Simulation of realistic atomistic models can provide a detailed picture of the evolution of thin film morphologies, and comparison with experiment facilitates determination of key energetic parameters.[11,13,15] However, this approach does not necessarily provide a clear elucidation of the subtle cooperative aspects of morphological evolution during film growth, e.g., the dynamics of mound steepening or coarsening. Instead, an alternative and effective strategy to achieve this goal is to analyze "step dynamics" models for film growth in which steps between discrete layers are regarded as having continuous lateral positions.[25] One must specify the propagation velocities of the steps, where often these are determined from a Burton-Cabrera-Frank (BCF) type[26] analysis of deposition, diffusion, and aggregation of atoms at step edges (although one can and here we do consider behavior for a more general class of models). This approach has been applied for simple cubic lattice geometries to address the classic problem of smoothing of rough films in the absence of deposition.[27,28] These constitute problems in nonequilibrium thermodynamics with evolution during smoothing being driven by minimization of the surface free energy. Of more relevance here are previous applications of this approach to study far-from-equilibrium film growth during deposition. Film growth often includes effectively irreversible processes (e.g., incorporation of diffusing adatoms at step edges), and thus evolution is determined by kinetic rather than thermodynamic factors. However, to date this step dynamics formulation has primarily been applied for the case of a simple cubic-lattice geometry in the absence of nonthermal downward transport near step edges.[29–34] Such models do not include any mechanism for mound slope selection during growth.

In this paper, we explore a class of step dynamics models incorporating both inhibited interlayer transport and downward funneling at step edges. These models, described in Sec. II, were introduced in a recent Letter,[35] and can be applied to describe the selection of mound slopes and shapes

during unstable multilayer growth. Comprehensive analysis of the evolution near the valley of a single semi-infinite mound in Sec. III reveals the occurence of slope selection. This behavior reflects the dynamics of step annihilation at the valley between mounds, which is in turn strongly influenced by DF. The variation of the selected slope with diffusion bias is fully characterized from such studies.

Application of step dynamics formulations to describe the evolution and shape selection of finite mounds in Sec. IV reveals that another key factor is the specification of the nucleation of islands (i.e., the creation of new steps) on the top of mounds. An early mean-field deposition-diffusion equation treatment of island nucleation on-top of other islands[36] identified the existence of a fairly well-defined critical radius for the supporting island R_{top} so that nucleation occurs on top when the growing island radius is close to this value. Subsequently, it was found that this analysis had to be corrected in the presence of a large ES barriers due to a breakdown of the traditional mean-field formulation.[37–39] The analysis was also refined to treat nucleation on top of a stack of islands representing a growing mound.[1] Nonetheless, the above picture of a fairly well-defined critical size survives. The corresponding deterministic picture of top layer nucleation was implemented to analyze the evolution of the shape of individual wedding-cake-like mounds in the presence of a large ES barrier.[31,38] A deterministic formulation of nucleation is also implemented in our analysis, but we also briefly comment on a more realistic stochastic formulation. Our simulations show how the prescription of nucleation affects the selected mound shape, particularly near the peak.

In Sec. V, further discussion of slope selection during mound formation is presented, as well as a comparison with the behavior predicted in phenomenological continuum treatments. We present our conclusions in Sec. VI.

II. STEP DYNAMICS MODELS INCLUDING DF

A. Model specification

Figure 1 illustrates the basic ingredients of the class of models which we consider for the step-flow dynamics of a staircase representing the side of a (1+1)D mound. For convenience, below all lateral positions and distances are measured in dimensionless units of lateral surface lattice constant. Also, in the following discussion, the mound valley is at $x=0$ and the peak is at $x=R$, so the mound corresponds to a staircase of steps increasing from left to right. The step n is located at $x=x_n$, where initially $1 \leq n \leq n^*$, so 1 and n^* label the bottom and top step, respectively. The width of the terrace n between step n and step $n+1$ is $L_n=x_{n+1}-x_n$, for $1 \leq n < n^*$. The width of the bottom terrace is $L_0=x_1$, and the width of the top terrace is $L_{n^*}=R-x_{n^*}$. Finally, the interlayer spacing is denoted by b, but we shall set $b=1$ in all numerical simulations.

We now fully specify the dynamics for these models. Atoms are deposited at rate F (in monolayers per unit time), diffuse across the terraces and incorporate irreversibly at steps subject to the influence of inhibited interlayer transport. As noted above, in contrast to standard step dynamics analy-
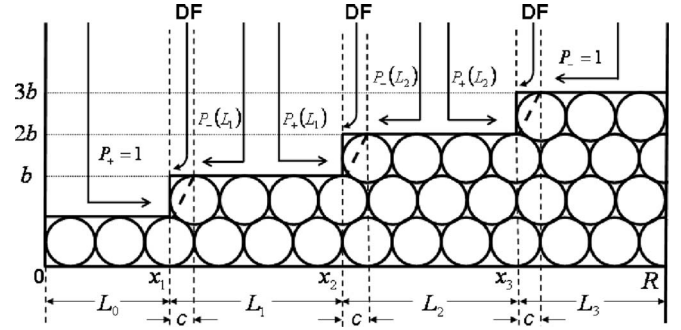
FIG. 1. Schematic of step dynamics models showing deposition, DF, and surface diffusion processes. $x=0(R)$ corresponds to the mound valley (peak), x_n the position of step n, and L_n the width of terrace n. $P_+(P_-)$ gives the probability of diffusing adatoms being incorporated at ascending (descending) steps. "Step edge regions" have width c.

ses, DF deposition dynamics is incorporated into these models. More specifically, atoms deposited in a "step edge region" within a distance c above each step are funneled downward and incorporate at that step as illustrated in Fig. 1. All atoms deposited on the bottom and top terrace aggregate to step 1 and step n^*, respectively. Atoms deposited on terrace $n(1 \leq n < n^*)$ outside of the step edge region either aggregate to the ascending step $n+1$ with probability $P_+(L_n)$, or to the descending step n with probability $P_-(L_n)$. Here, in general, these probabilities can depend on the terrace width L_n, but they must satisfy the constraint $P_++P_-=1$. The presence of inhibited interlayer transport implies an uphill diffusion bias with strength $P_+-P_-=\Delta>0$. Below, t will denote the deposition time, and thus $\theta=Ft$ will denote the coverage or film thickness in units of monolayers (ML).

We should emphasize that these step dynamics models are well defined and can be analyzed for a broad class of choices of the dependence of $P_{\pm}(L)$ on terrace width L, subject to the above constraints. However, the basic behavior of mound slope and shape selection should be independent of the specific choice of this L dependence. One natural choice might be guided by a BCF-type formulation where one solves the continuum deposition-diffusion equation on each terrace for irreversible incorporation at ascending steps with no barrier and at descending steps with a finite ES barrier, δ. This analysis, which applies for $L \gg 1$, suggests an L dependence of the form[1]

$$P_+(L) = \frac{1/2 + L_{ES}/(L-c)}{1 + L_{ES}/(L-c)}. \tag{1}$$

Here $L_{ES}=\exp[\delta/(k_BT)]-1$ is the ES length (assuming equal prefactors for intralayer and interlayer hopping), k_B is Boltzmann's constant, and T is the surface temperature. However, given our view that basic model behavior should be independent of the choice of L dependence, we primarily consider the simplest case where the $P_{\pm}$ are set constant.

B. Evolution equations

The total flux of atoms reaching step n determines the velocity V_n of that step. Accounting for the different behavior

indicated above for the bottom step $n=1$, steps in the interior of the staircase $1<n<n^*$ and the top step $n=n^*$, one obtains

$$\frac{dx_1}{dt} = V_1 = -FL_0 - F(L_1-c)P_-(L_1) - Fc, \qquad (2)$$

$$\frac{dx_n}{dt} = V_n = -F(L_{n-1}-c)P_+(L_{n-1}) - F(L_n-c)\mathrm{P}_-(L_n) - Fc, \qquad (3)$$

$$\frac{dx_{n^*}}{dt} = V_{n^*} = -F(L_{n^*-1}-c)P_+(L_{n^*-1}) - F(L_{n^*}-c) - Fc. \qquad (4)$$

On the right-hand side (RHS) of each equation, the first (second) term corresponds to diffusive flux from the terrace to the left (right) of that step, and the third term is the DF flux. Note that setting $c=0$ recovers a step dynamics model without DF.

One particularly significant observation regarding the evolution equation for the widths L_n of *interior* terraces is that all terms involving c (including DF terms) cancel out exactly for constant $P_\pm$. Partial cancellation persists for general $P_\pm$. Even so, DF will still dramatically influence mound slope selection as shown later, noting that DF terms persist in the evolution equations for the widths of the bottom and top terraces.

Evolution of the steps and terraces in mound formation can be analyzed by integrating the above equations with special treatment of the bottom and top steps. During deposition, the bottom steps will disappear or annihilate, and the top steps will be created by nucleation of new top layer islands as shown in Fig. 2. For the bottom step, Eq. (2) is only integrated until a time $t=t_1$, say, when x_1 reaches zero. At this time step 1 disappears, and step 2 becomes the bottom step. Consequently, the equation for step 2 is updated from type (3) to type (2), then integrated until time t_2 when x_2 reaches zero, etc.

Previous studies of step dynamics models without DF ($c=0$) described the treatment of steps at a mound valley, primarily for the special case where $P_+=1$ (no interlayer transport).[29] Here, since $dx_1/dt=-Fx_1$, it follows that the bottom step never vanishes, so that the height of the valley is stationary, and a deep groove develops near the valley. This fixed valley height is an artifact of the continuum decription[29] which disappears in an atomistic treatment. However, a deep groove persists in models without DF even for $P_+<1$. We will see that this type of behavior does not occur with DF ($c>0$).

At the mound peak, new top layers are created by island nucleation. At a prescribed time of nucleation $t=t'_{n^*+1}$, we introduce a new step n^*+1 with position $x_{n^*+1}=R$, and update the equations appropriately.[40] In our modeling, we invoke a deterministic prescription of nucleation: a new top layer island is created when the width of the top terrace reaches some specified critical value R_{top}. However, the basic results remain unchanged if one implements a more realistic stochastic prescription. See Appendix A.
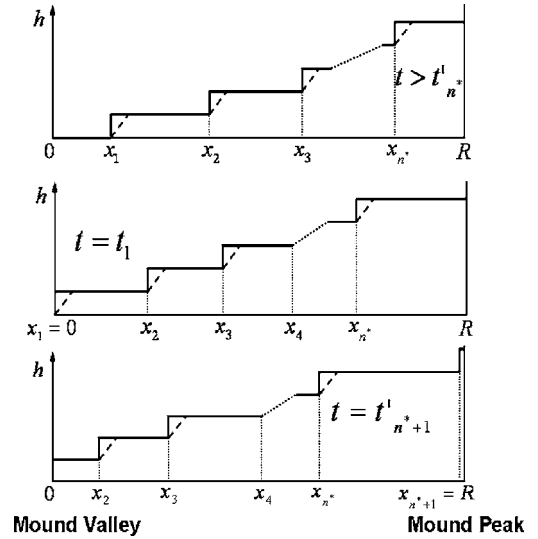
FIG. 2. Schematic showing the disappearance of the bottom steps at the mound valley, and the nucleation of new top layer islands (i.e., islands at the mound peak), during deposition. Consistent with the more detailed Fig. 1, the dashed diagonal line at each step indicated the "step edge region" in which DF occurs. For deterministic nucleation, $x_{n^*}=R-R_{\mathrm{top}}$ in the bottom frame.

C. Net step attachment flux

For elucidation of the behavior of these step dynamics models, our initial study[35] indicated the value of analyzing a suitably defined net mass flux of adatoms attaching to steps, summing contributions across the side of a mound between its valley and peak. More precisely, to obtain this total net flux which will be denoted below by K_{tot}, we sum over fluxes accumulating at all steps from the left, and subtract the sum over fluxes accumulating at all steps from the right. We now identify the different contributions to this total flux. The net diffusive flux across the terrace n for $1\leqslant n<n^*$, $K_n=+F(L_n-c)[P_+(L_n)-P_-(L_n)]>0$, is uphill. The flux across the bottom terrace where all atoms reach step 1, $K_0=+FL_0>0$, is also uphill. In contrast, the flux across the top terrace, $K_{n^*}=-F(L_{n^*}-c)<0$, is *downhill*. In addition, there is a downhill current from DF of $K_{\mathrm{DF}}=-Fc$ at each step. All of these contributions must be added to obtain $K_{\mathrm{tot}}=\Sigma_{0\leqslant n\leqslant n^*}K_n+n^*K_{\mathrm{DF}}$. For constant $P_\pm$, after naturally rescaling by the deposition flux and the mound radius, one obtains the simplified formula

$$\hat{K}_{\mathrm{tot}} = K_{\mathrm{tot}}/(FR) = (P_+ - P_-) + 2P_-(x_1/R) - 2P_+(L_{n^*}/R) - 2P_+c(n^*-1)/R. \qquad (5)$$

The following key features should be noted.[35] During the "steady-state evolution" of selected mound shapes, $\hat{K}_{\mathrm{tot}}$ is nonvanishing, varying periodically for deterministic nucleation (with the period of 1 ML). However, the mean value $\langle\hat{K}_{\mathrm{tot}}\rangle$, of $\hat{K}_{\mathrm{tot}}$ time averaged over the period of 1 ML does exactly vanish. This condition was shown to directly constrain the selected mound shapes[35] See below.

III. EVOLUTION OF SEMI-INFINITE MOUNDS

In this section, we use the step dynamics model to investigate the evolution of semi-infinite mounds focusing on behavior near the valley between mounds. In such an analysis, we eliminate the dependence of mound evolution on the prescription of top layer nucleation. Thus, it is possible to cleanly extract the influence of the prescription of behavior at the mound valley (anticipating that the basic features may persist in the more complicated case of finite mounds). The general step dynamic equations are the same as Eq. (3), except that now $n^* \to \infty$. For constant $P_\pm$, the evolution equations for a semi-infinite mound can be written as

$$\frac{dx_1}{d\theta} = -L_0 - L_1 P_- - cP_+, \tag{6}$$

$$\frac{dx_n}{d\theta} = -L_{n-1}P_+ - L_n P_-, \quad \text{for } n > 1. \tag{7}$$

Here, we use the natural coverage variable $\theta = Ft$. We note the parameter c does not appear in Eq. (7). Furthermore, there exists a class of solutions to these equations having a simple scaling behavior with respect to the parameter c. Specifically, if $\tilde{x}_n(\theta)$ represents a set of solutions for $c = 1$, then $x_n(\theta) = c\tilde{x}_n(\theta)$ provides corresponding solutions for general c.

A. General and periodic solutions for a model with DF: Numerical analysis

In our analysis of the above equations for a semi-infinite mound, we set up an initial mound configuration where all terraces have equal width, L_∞. Then, far from the mound valley where $n \gg 1$, one has that $L_{n-1} \approx L_n = L_\infty$, and Eq. (7) can be written as

$$\frac{dx_n}{d\theta} \approx -L_\infty, \tag{8}$$

so that $x_n \approx x_n^0 - L_\infty \theta$. Therefore, all such steps move with the same constant velocity preserving the equal terrace width far from the mound valley. However, distinct evolution and annihilation of steps at the mound valley induces a disruption of this equal step spacing, an effect which propagates away from the mound valley.

In our numerical analysis, we integrate Eq. (6) and (7) initially for $1 \leq n < n_c$, where n_c is some large cutoff and where we set $L_{n_c} = L_\infty$. When x_1 becomes zero, and the bottom step disappears, an additional step $n_c + 1$ at position $x_{n_c+1} = x_{n_c} + L_\infty$ is introduced, and we set $L_{n_c+1} = L_\infty$. Now L_{n_c} is determined from the evolution equations.

Figure 3 shows the evolution of a semi-infinite mound with DF for the different choices of initial mound slope $m_\infty = b/L_\infty$. Here, we set $P_+ = 0.52$, $b = 1$, and $c = 1/2$. Choosing an initially "steep" slope of the mound leads to flattening at the base. Choosing an initially "shallow" slope leads to steepening at the base. In general, a region with a unique selected value of slope, m_s^∞, develops at the base of the mound and spreads outward.

Next, we use the determined value of m_s^∞ as the initial slope to provide a detailed characterization of the evolution
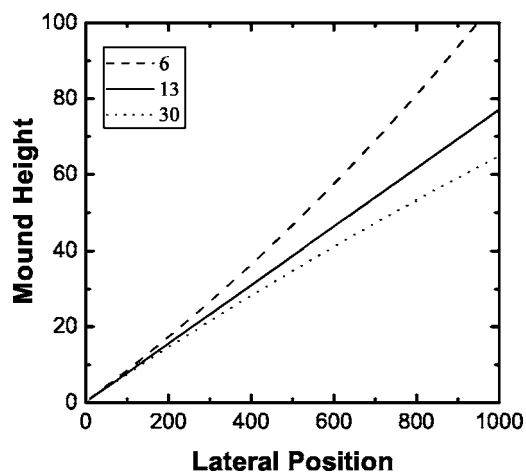
FIG. 3. Evolution shapes of semi-infinite mounds with DF for $c = 1/2$, $b = 1$, and $P_+ = 0.52$. Behavior is shown for various choices of the initial terrace width $L_\infty = 6$, 13, and 30. The selected terrace width is $L_s \approx 13$.

of semi-infinite mounds with selected slope. Figure 4 shows the evolution of the widths of the lowest five terraces with coverage for various P_+. After a brief transient period lasting only a couple of ML, the evolution of this semi-infinite mound reaches a "steady-state" regime. More precisely, evolution becomes periodic (in the reference frame moving upwards with the growing film) with a period of one ML. The width of the lowest terrace varies dramatically with time, noting that this terrace periodically disappears. The variation of the width of the second lowest terrace is not as great, but is still quite significant. The variation of the terrace width fades away for terraces increasingly further from the mound valley.

Finally, results for m_s^∞ versus Δ with $c = 1/2$ are shown in Fig. 5. Behavior for general c follows immediately using the scaling relation described above.

B. Periodic solutions for a model with DF: Approximate analytic treatment

Here, we discuss analytic treatment of the periodic solutions for a semi-infinite mound. In principle, one could
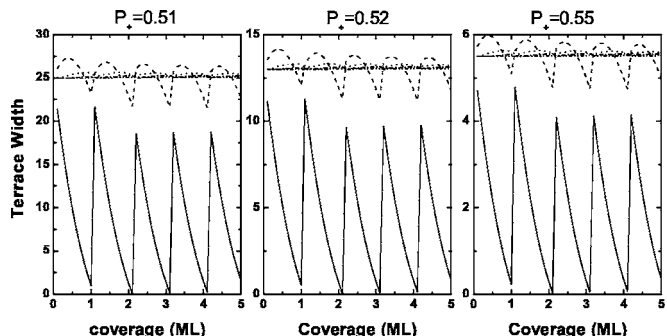
FIG. 4. Variation of width of the first five terraces with coverage for evolution of a semi-infinite mound with DF which has initially equal width terraces consistent with the selected slope. The magnitude of the variation in time decreases monotonically for steps further from the base of the mound. Here, $c = 1/2$ and $b = 1$. (a) $P_+ = 0.51$, (b) $P_+ = 0.52$, (c) $P_+ = 0.55$.
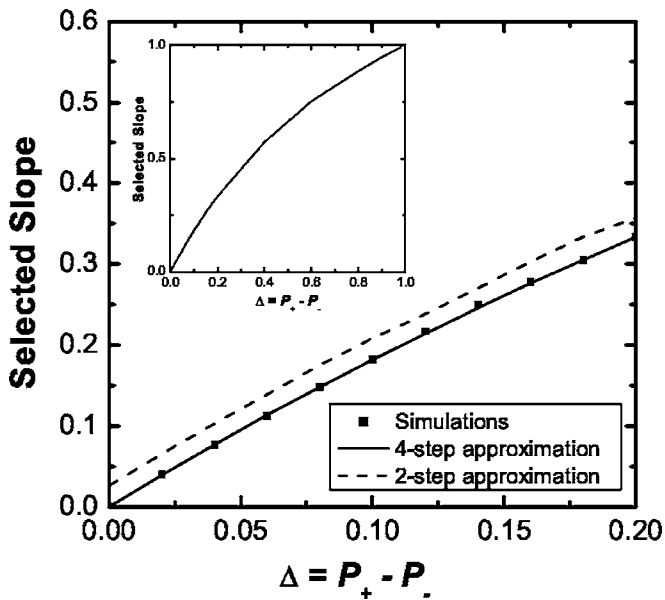
FIG. 5. Variation of the selected slope with smaller Δ obtained from simulations of step dynamics model (with $b=1$ and $c=1/2$), and from analytical calculations within the two- and four-step approximations. The inset shows the precise full Δ dependence.

search for periodic solutions to the set of semi-infinite linear equations (6) and (7). This is likely only viable for constant $P_\pm$ as one can perform a spectral analysis for the associated infinite-dimensional linear evolution operator. Such an analysis of the semi-infinite set of equations is provided in Appendix B for the simple case where $P_+=1$. However, with minimal approximation, it is possible to reduce the semi-infinite set of evolution equations to a finite linear set which can be analyzed much more simply (for general P_+).

The most severe (but still reasonable) approximation neglects the variation in time of the widths of terraces other than the bottom two, L_0 and L_1. Specifically, we set

$$L_2 = L_3 = L_4 = \cdots = L_\infty (\text{const}) \tag{9}$$

for the periodic evolution of the semi-infinite mound with selected slope. Then, we must analyze just two equations for the bottom step and the second step, which for constant $P_\pm$ have the form

$$\frac{dx_1}{d\theta} = -P_+ x_1 - P_- x_2 - P_+ c, \tag{10}$$

$$\frac{dx_2}{d\theta} = -P_+(x_2 - x_1) - P_- L_\infty \tag{11}$$

but subject to temporal boundary conditions corresponding to a periodic solution. If one specifies that $\theta=0$ corresponds to the time just after the bottom step disappears, and at this time one specifies the position of the "new" bottom step as $x_1(\theta=0)=x^*$, then it follows that $x_2(\theta=0)=x^*+L_\infty$. After one ML deposition, the positions of x_1 and x_2 must satisfy

$$x_1(\theta=1) = 0 \quad \text{and} \quad x_2(\theta=1) = x^*. \tag{12}$$

Equation (10) and (11) can be solved analytically subject to the specified initial conditions. Satisfying the two constraints in Eq. (12) determines the two unknowns x^* and $L_\infty = b/m_s^\infty$. Corresponding results for the selected slope for $c=1/2$ shown in Fig. 5 accurately describe the quasilinear variation of m_s^∞ with weaker diffusion bias, Δ, but include a small offset.

The small offset or error in the above approximation for m_s^∞ derives from the feature that the neglected variation in L_2 is significant. It is certainly much larger than that of L_3, $L_4, \ldots$. Thus, we consider a much more accurate treatment where we allow L_2 and L_3 to vary in addition to L_0 and L_1.[41] Here, we retain four equations for x_1, x_2, x_3, and x_4, and specify initial conditions $x_1(0)=x_1^*$, $x_2(0)=x_2^*$, $x_3(0)=x_3^*$, and $x_4(0)=x_3^*+L_\infty$. These equations are solved subject to the constraints for a periodic solution that $x_1(1)=0$, $x_2(1)=x_1^*$, $x_3(1)=x_2^*$, and $x_4(1)=x_3^*$. This yields four equations for four unknowns including $L_\infty = b/m_s^\infty$. Results for $c=1/2$ shown in Fig. 5 for m_s^∞ agree almost perfectly with the numerical results. More generally, this approximation accurately recovers the full periodic evolution of the terrace widths close to the mound base.

For the case with no interlayer transport, $P_+=\Delta=1$, the periodic solution for a semi-infinite mound can be analyzed exactly and completely (including the nontrivial behavior near the base of the mound). In particular, this analysis yields $m_s^\infty = b/(2c)$. See Appendix B.

It should be noted that both these approximations preserve the exact scaling behavior $m_s^\infty \propto b/c$ for constant $P_\pm$. A more comprehensive analysis using the precise four-step approximation reveals a crossover from the quasilinear variation $m_s^\infty \approx (b/c)\Delta$ for smaller Δ, to the limiting behavior $m_s^\infty = b/(2c)$ for $\Delta=1$. In the inset to Fig. 5, we present results for $c=1/2$. Finally, we mention that Politi[42] has determined the exact behavior of m_s^∞ versus Δ for the step dynamics model with DF. His result follows from the condition, $\langle \hat{K}_{\text{tot}} \rangle = 0$, on the net step attachment flux mentioned in Sec. II C after letting $R \rightarrow \infty$.

C. Comparative analysis for a model without DF ($c=0$)

It is instructive to directly compare the evolution of semi-infinite mounds with and without DF, choosing the initial slope in both cases to match the selected slope m_s^∞ for the model with DF. While the evolution of a mound with DF quickly converges to a nearly linear shape, a deep groove develops at the valley of the mound without DF. See Fig. 6. The difference between these two cases can be attributed to the very different rate of upward motion of the mound valley. This rate is strongly influenced by the presence of DF which facilitates annihilation of the bottom step (and corresponding increase of this height by one layer). The formation of a deep groove for the case without DF ($c=0$) is the well understood "Zeno effect," and has been analyzed in detail.[29,30] One can show that the terrace width distribution as a function of film height satisfies a simple diffusion equation,[35] and is thus described by the tail of an erf distribution in the vicinity of the groove.[29]
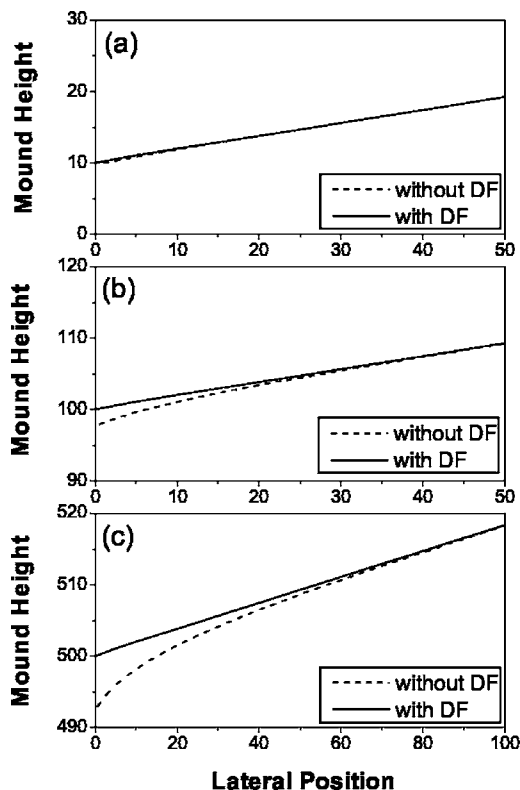
FIG. 6. Comparison of the evolution shape of a semi-infinte mound with DF ($c=1/2$) and without DF ($c=0$) at different coverages: (a) 10, (b) 100, and (c) 500 ML. Here, we set $P_+=0.55$, and $b=1$.

IV. EVOLUTION OF MOUNDS WITH FINITE SIZE

In this section, we use our step dynamics model to analyze the evolution of a mound with finite size. A deterministic prescription for nucleation is implemented: a new top layer island is created when the width of the top terrace reaches a prescribed critical value R_{top}.

A. Mound evolution for a model with DF

Our main focus in this work is on selected mound shapes and slopes. However, our step dynamics model can also be used to assess evolution of mound shapes prior to shape selection. Such transient evolution is generally significant for large ES barriers, where the selected slope is large and where initial evolution is not greatly impacted by slope selection. Indeed, in metal(111) homoepitaxial systems, the presence of large ES barriers and low terrace diffusion barriers produces mounds with large bases for which there is a prolonged regime of mound steepening.[38] The transient evolution of the wedding-cake-like mounds in such systems has been successfully described using a step dynamics model without DF, and for which there is no steady-state selected shape.[31,32,38] However, ultimately real growth systems must display a crossover to "steady-state" behavior reflecting a selected slope. [It is less well appreciated that extended regimes of mound steepening can also occur in metal(100) homoepitaxy with low ES barriers.[11]]
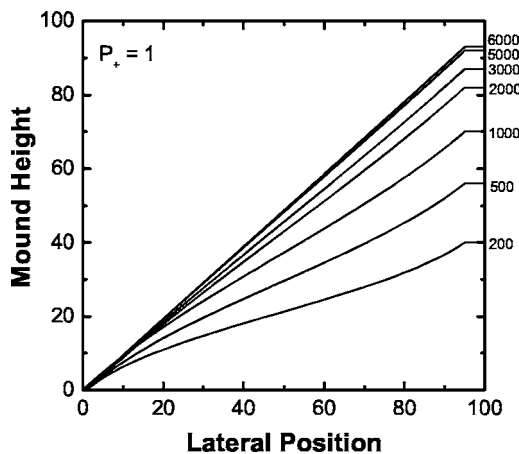
FIG. 7. Transient evolution and asymptotic selection of mound shapes for $P_+=1$ and $c=1/2$. Here, we set $R=100$, $R_{top}=5$, and $b=1$. The number on the right side indicates the corresponding coverage for each mound shape.

To explore this issue, we monitored the evolution of a mound with DF for $c=1/2$ with $P_+=1$ (no diffusive interlayer transport). Figure 7 shows the mound shapes at different times for a mound with $R=100$ and $R_{top}=5$. Indeed, after an initial transient regime of few thousand ML with progressive steepening of the mound, there is a crossover to a rather distinct selected shape.

B. Mound shape selection for a model with DF

Next, we focus on characterization of selected mound shapes in the general case of inhibited interlayer transport. Figure 8 shows the selected mound shapes after a long-time evolution obtained from the analysis of the step dynamics model based on Eq. (2)–(4) with $P_+=0.55$ and $c=1/2$ for the various choices of R_{top}. Clearly, mound shapes are strongly influenced by the prescription of nucleation: facile nucleation (corresponding to small R_{top}/R) produces narrow terraces and pointed mound peaks; inhibited mound nucleation (corresponding to large R_{top}/R) produces a significantly flattened mound peaks.
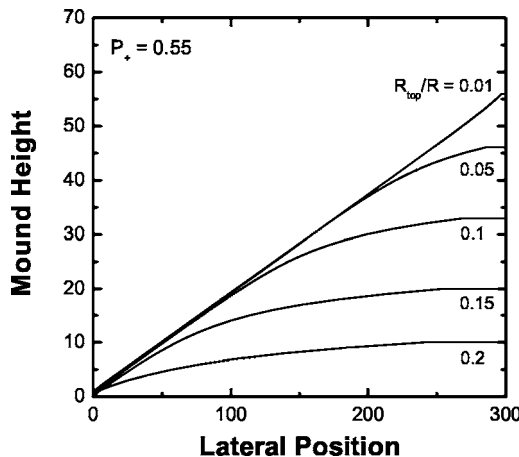
FIG. 8. Selected mound shapes for a model with DF ($c=1/2$) and various choices of R_{top}. Here $P_+=0.55$, $R=300$, and $b=1$.
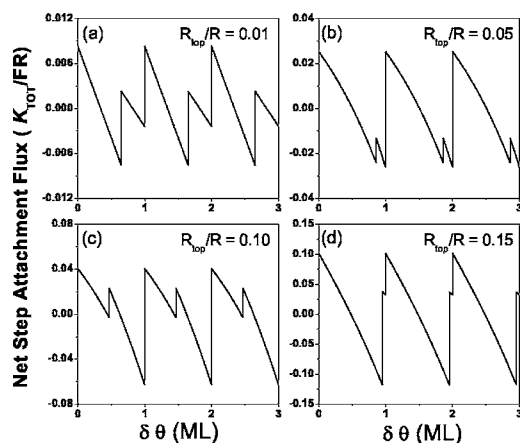
FIG. 9. Periodic variation of the net step attachment flux $\hat{K}_{tot}$, with coverage increment $\delta\theta$ in the "steady-state" of model with DF ($c=1/2$). Behavior is shown for different R_{top}. R_{top}/R = 0.01 (a), 0.05 (b), 0.10 (c), and 0.15 (d), respectively. Here $P_+=0.52$ and $R=1000$.

For smaller R_{top}/R, a region with well-defined selected slope, m_s, emerges at least near the mound base. Furthermore, this slope corresponds to the value of m_s^∞ obtained in the above analysis of semi-infinite mounds. For larger R_{top}/R, the shape of the entire mound is impacted by top-layer nucleation, and no well-defined selected slope appears (although the details of the shape are still strongly influenced by DF).

The above discussion considers only a deterministic prescription of nucleation. Thus, it is appropriate to ask what features are preserved for a more realistic stochastic prescription of nucleation as described in Appendix A. With stochastic nucleation, evolution is no longer periodic. However, if one averages over many ML of deposition, one expects to find a well-defined mound shape with a smooth peak. Our analysis shows that using stochastic rather than deterministic nucleation produces at most a slight change in mound shape near the peak.

C. Net step attachment flux across the mound side

To further elucidate the selection of mound shapes, it is instructive to analyze the behavior of the net step attachment flux, $\hat{K}_{tot}$, defined in Sec. II B. The long-time solution to Eqs. (2), (3), (4) for selected mound shapes in the model with DF is not time invariant. Rather, it is periodic in the reference frame of the growing film with period of 1 ML. Thus, $\hat{K}_{tot}$ also varies periodically as shown in Fig. 9. Just after nucleation of a top layer island, downhill contribution from the top terrace is almost zero as the width of this terrace is negligible. Thus, $\hat{K}_{tot}$ as determined from Eq. (5) with $L_{n^*}=0$ is expected to be *positive*, since also the net uphill flux on other terraces should dominate the DF flux. As the top terrace grows, the downhill flux across it also grows and subsequently dominates the uphill contributions. Thus, at some point $\hat{K}_{tot}$ becomes negative. In particular, $\hat{K}_{tot}$ as determined from Eq. (5) with $L_{n^*}=R_{top}$ is negative just before a new

layer is created. After the new top layer is created, it jumps by an amount $(1+\Delta)(R_{top}/R)$ to recover its initial positive value decribed above.

There is also a jump within each period (in between top layer creation) which corresponds to the disappearance of the bottom step. Just after the disappearance of this step, a broad bottom terrace is created upon which all depositing atoms are incorporated at the step to the right and create a significant uphill flux. Thus, $\hat{K}_{tot}$ jumps to a more positive value at this point.

Our *key finding* is that the mean value of $\hat{K}_{tot}$ averaged over 1 ML always vanishes (when $c>0$) for deterministic nucleation. The impact of this condition on selected shape can be seen most clearly using Eq. (5). We consider only the typical case of mounds containing many steps where the maximum width of the bottom terrace is far smaller than the mound radius, so $x_1/R\ll 1$. Also, for selected shapes, the mound height $\delta h\approx bn^*$ or $b(n^*-1)$ (from valley to peak) is roughly constant. Then, setting $\alpha=L_{n^*}/R_{top}$, the condition $\langle\hat{K}_{tot}\rangle=0$ implies that

$$(P_+ - P_-) - 2P_+(R_{top}/R)\langle\alpha\rangle - 2P_+(c/b)(\delta h/R) = 0, \quad (13)$$

where $\langle\alpha\rangle\approx 1/2$ denotes the time average of α. Eq. (13) reflects a balance between the three main contributions to the total step attachment flux from the net uphill flux due to diffusion bias, and from the downhill fluxes due to diffusion across the top terrace and due to DF. It is immediately clear that, e.g., inhibited nucleation (i.e., larger R_{top}/R) implies less high mounds. This condition has been successfully applied to provide a boundary condition for continuum evolution equations derived from coarse-graining of the step dynamics equations.[35]

As an aside, a detailed analytic investigation of $\hat{K}_{tot}$ is presented in Appendix C for the extreme case where R_{top} is sufficiently large that there are at most two steps during periodic mound evolution. Finally, for stochastic nucleation, if one averages over many ML of deposition, one expects that the averaged $\hat{K}_{tot}$ again effectively vanishes. In this respect, the constraint on the net step attachment flux is preserved.

D. Evolution of a finite mound without DF

Step dynamics models without DF have been applied previously to analyze mound evolution, both the steepening of individual wedding-cake-like mounds with no interlayer transport,[31,32] and the evolution of quasiperiodic arrays of mounds with a finite ES barrier.[30] For the latter, mound steepening with the development of deep grooves at mound valleys was observed for larger wavelengths. However, a transition to "steady-state" evolution was observed with decreasing wavelength.[30]

Motivated by the latter, we consider the evolution of a single half-mound (representing a half period in a periodic array of mounds). Our analysis without DF implements deterministic nucleation and considers behavior for fixed mound radius R but various choices of R_{top} (rather than changing the period of $2R$). For sufficiently small R_{top}/R, we find that a deep groove develops at the mound valley, analo-
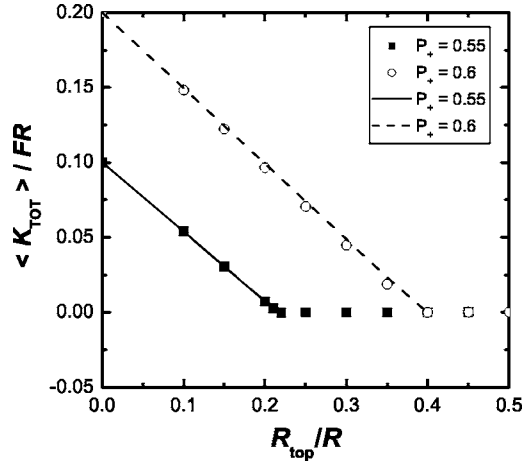
FIG. 10. Dependence on R_{top}/R of the mean value of $\hat{K}_{tot}$ averaged over 1 ML for the evolution of a mound without DF. Symbols and (solid or dashed) lines represent the results from step dynamics model and Eq. (14), respectively.

gous to behavior found in Ref. 30 for large wavelengths. However, if R_{top}/R is larger than a well-defined critical value r_c then the mound evolves to a "stationary" shape. This behavior is analogous to that found in Ref. 30 for short wavelengths. Note that r_c increases with increasing diffusion bias Δ.

Here, we provide further insight into this transition by again considering the behavior of the net step attachment flux across the mound side $\hat{K}_{tot}$. For R_{top}/R below the critical value r_c corresponding to persistent roughening of the mound, we find that the mean value $\langle \hat{K}_{tot} \rangle$, averaged over a period of 1 ML is strictly positive. (This value depends somewhat on the time when the averaging is performed as the mound is continually steepening.) In contrast, $\langle \hat{K}_{tot} \rangle$ vanishes for steady-state evolution when R_{top}/R exceeds r_c. See Fig. 10. Of course, for this model, there is no negative contribution to K_{tot} from DF. Thus, the negative contribution to K_{tot} which is responsible for the vanishing of the mean value when R_{top}/R exceeds r_c comes entirely from diffusion in the downhill direction across the top terrace.

An approximate but reasonable estimate of $\langle \hat{K}_{tot} \rangle$ and r_c comes from applying Eq. (5) with $c=0$ and neglecting the term including x_1. For smaller R_{top}/R, we found from the analysis of step dynamics model that $\langle L_{n^*} \rangle \approx 0.42 R_{top}$. Then, Eq. (5) becomes

$$\langle \hat{K}_{tot} \rangle \approx \Delta - 0.42(1+\Delta)(R_{top}/R) \qquad (14)$$

for $R_{top}/R \lesssim r_c$ with $r_c \approx 2.38\Delta/(1+\Delta)$. Finally, we note that although a stationary shape is obtained for R_{top}/R above the critical value r_c there is no tendency for slope selection (without DF).

V. MOUND SHAPE AND SLOPE SELECTION IN PHENOMENOLOGICAL CONTINUUM TREATMENTS

Mound slope selection and subsequent evolution have been modeled extensively using phenomenological con-

tinuum theories (PCTs). In these PCTs for $(1+1)$D, the evolution of a continuous film height $h(x,t)$ at lateral position x and time t, obeys[1,8,12,30,43–47]

$$\frac{\partial}{\partial t}h(x,t) = Fb - \frac{\partial}{\partial x}J_{PCT}(x,t). \qquad (15)$$

where J_{PCT} is a suitable mesoscale or coarse-grained lateral mass current which is proportional to F (assuming no desorption and irreversible incorporation at step edges). It is an open and challenging problem to rigorously derive an expression for J_{PCT} starting from an atomistic model. Typically, a phenomenological form is assumed where J_{PCT} is decomposed as $J_{PCT}=J_{up}+J_{DF}+J_{SB}+J_{relax}$.

Here, $J_{up}(m)$, which depends on the local slope $m=\frac{\partial}{\partial x}h$, denotes the destabilizing net uphill current due to surface diffusion in the presence of inhibited interlayer transport.[1,5] $J_{DF}(m)$ denotes the downhill current due to DF. In the "simplest picture,"[48] it is taken as the microscopic lateral downhill current associated with DF which is proportional to the step density, and thus to m.[15,49–53] The term J_{SB} produces up-down symmetry breaking, and J_{relax} facilitates "relaxation" near mound peaks and valleys.[8,30] Shape selection in the PCT corresponds to the vanishing of J_{PCT}. For selected slopes on the straight sides of mounds (where both J_{SB} and J_{relax} vanish), this corresponds to cancellation of the J_{up} and J_{DF}.

A simple estimate of the dominant behavior of J_{UP} for broader terrace widths $L=b/|m|$ significantly greater than c (but still in the step flow regime) would suggest that $J_{up}(m) \approx Fb\Delta L/2$. A refined estimate from coarse-graining of step dynamics equations for local stair-case regions yields $J_{up}(m) \approx Fb\Delta(L-c)/2$.[35] In either case, assuming that $J_{DF} \propto m$ leads to the result $m_s^{PCT} \approx (b/c)\sqrt{\Delta}$, for small Δ. This apparent discrepancy with the predicted linear variation in the step dynamics model was noted previously,[35] but is misleading.

We now present a more detailed and precise analysis of the relevant microscopic lateral mass currents in our model (based on the mean lateral distance travelled per depositing atom due to specific processes) for atoms depositing on a perfect staircase with terrace width L. For DF, the fraction of atoms deposited in the step region is c/L, and mean lateral distance traveled by those atoms deposited is $c/2$. Thus, one has that

$$J_{DF}(m) = -Fb(c/2)(c/L) = -Fc^2m/2. \qquad (16)$$

Next, consider the remaining fraction $(L-c)/L$ of atoms deposited on a terrace of width L outside the step edge region. Those attaching to the accending step (with probability P_+) travel an average distance of $(L-c)/2$. Those attaching to the descending step (with probability P_-) travel an average distance $c+(L-c)/2=(L+c)/2$ accounting for the extra nondiffusive motion across the step region. Thus, one has

$$J_{up}(m) = Fb[P_+(L-c)/2 - P_-(L+c)/2](L-c)/L$$

$$= Fb\Delta(L-c)/2 - Fbc(L-c)/(2L). \qquad (17)$$

Setting $J_{up}(m)+J_{DF}(m)=0$ to obtain the selected slope

$m = m_s$ yields exactly the same result as obtained from the step dynamics modeling, i.e., $m_s^{PCT} \approx (b/c)\Delta$, for small Δ, crossing over to $m_s^{PCT} = b/(2c)$, for $\Delta = 1$.

There have been several simulation-based and analytic studies of slope selection for realistic astomistic models of homoepitaxial growth (effectively corresponding to a BCF-type rather than a constant choice of $P_\pm$).[15,23,49,51–53] These determined net lateral mass current, J_{PCT}, and even separate contributions, based on the above microscopic definition, i.e., from the mean lateral distance traveled per deposited atom. These analyses of selected slope are thus consistent with that above.

There remains the challenge of developing reliable expressions for J_{PCT} in the evolution equation for a PCT. One strategy is to first obtain a "local" continuum evolution equation by coarse graining of the step dynamics model over a single mound. This produces a J_{PCT} without any DF or relaxation terms, and which is nonvanishing over a single mound of selected shape.[35] This is not inconsistent with the boundary conditions applied at the mound valley (which imposes the selected slope) and at the peak. In any case, one could add or subtract a constant to J_{PCT} without changing evolution. For the desired further-coarse grained evolution equation applicable for arrays of mounds, we are exploring the replacement of the boundary condition at the peak by effective relaxation term.[35] One must also reliably treat slope selection and behavior near the mound valleys.

VI. DISCUSSION AND CONCLUSIONS

We have shown that refinement of conventional step dynamics models incorporating downward funneling (DF) deposition dynamics is a particularly effective tool for elucidation of mound shape and slope selection during unstable multilayer growth. Our analysis reveals how the incorporation of DF (or other nonthermal downward transport mechanisms) leads to slope selection. A key effect of DF is to facilitate step annihilation at the mound valleys and thus to enhance the growth of the valley heights at the base of mounds.

A key concept in analysis of these step dynamics models is the net step attachment flux K_{tot} and the associated constraint $\langle K_{tot} \rangle = 0$, which controls selected mound shapes. It is natural to compare this picture with the steady-state condition in PCT that the coarse-grained lateral mass current vanishes, i.e., that $J_{PCT} = 0$. There is of course some similarity between K_{tot}, or its local components K_n and K_{DF}, and J_{PCT}. Indeed, we have shown consistency in the prediction of selected slopes from these two formulations. However, only K_{tot} is defined precisely and generally for the discrete step dynamics model, and only this quantity varies periodically alternating in sign (with significant amplitude for larger R_{top}/R).

Key concepts (e.g., related to K_{tot}) and analytic techniques (e.g., for analysis of periodic solutions) developed or utilized in this work have general applicability beyond the case of constant $P_\pm$ (for which we presented simulation results). As indicated in Sec. II, it is natural to consider a BCF-type choice of $P_\pm$ as given in Eq. (5), which should be applicable at least in the regime of broader terraces or smaller slopes. In our step dynamics model with DF for this choice, now a key parameter is the rescaled ES length $l_{ES} = L_{ES}/c$. Analysis of the selected slope for this model reveals a transition from smooth growth for $l_{ES} < 1$ (where effectively $m_s = 0$) to mound formation with m_s increasing linearly (in l_{ES}) from zero for $l_{ES} > 1$ and quickly saturating at a maximum value for $l_{ES} = O(1)$. These observations have consequences for interpretation of experiments. For example, the small mound slopes observed in experimental and simulation-based studies of the growth of Ag on Ag(100) at 300 K may not correspond to true selected slopes since l_{ES} is likely significantly larger than unity.[11] Instead, the observed slopes may be controlled by a relatively large value of R_{top}/R for this system.

APPENDIX A: STOCHASTIC NUCLEATION

In the deterministic nucleation scheme used above, a new terrace or island is created on the top of a mound exactly when the radius of the current top terrace reaches a critical value of R_{top}. In reality, the nucleation occurs for a distribution of radii centered on such a "critical" value. Thus, a more realistic stochastic prescription of nucleation could be implemented based on a knowledge of this distribution.

Detailed analysis of the nucleation process on top of mounds indicates that the probability for *no nucleation* to have occurred is given by[1,2]

$$P_{nonuc}(t) = \exp\left[-c_n \left(\frac{R_{isl}(t)}{R_{top}} \right)^n \right], \qquad (A1)$$

where $R_{isl}(t)$ is the growing radius of the top island at a time t after its nucleation. The choice of the constant c_n will be described below. The value of the exponent n depends on the strength of the ES barrier. Adapting the existing analyses[1] to $(1+1)$D, one can show that $n = 5$ for $L_{ES} \gg L_{isl}$, and $n = 6$ for $L_{ES} \ll L_{isl}$ for the $(1+1)$D models described here. Different values are obtained for $(2+1)$D models.[54]

If $p_{nuc}dt$ describes the probability for nucleation to occur between times t and $t+dt$, then it follows that

$$p_{nuc}(t) = \frac{d}{dt}(1 - P_{nonuc}), \quad \text{where} \int_0^\infty p_{nuc}(t)dt = 1.$$

$$(A2)$$

More usefully, if $p_{nuc}^* dR_{isl} = p_{nuc}dt$ describes the probability for nucleation to occur when the island radius is between R_{isl} and $R_{isl} + dR_{isl}$, it follows that
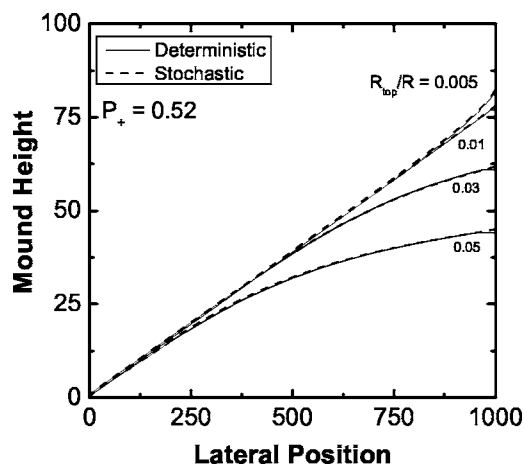
FIG. 11. Comparison of the deterministic and stochastic nucleation schemes. Here, we choose $n=6$, $c=1/2$, and $b=1$.

$$p_{\text{nuc}}^*(R_{\text{isl}}) = nc_n \frac{(R_{\text{isl}})^{n-1}}{(R_{\text{top}})^n} \exp\left[-c_n\left(\frac{R_{\text{isl}}}{R_{\text{top}}}\right)^n\right]. \qquad \text{(A3)}$$

This distribution is quite sharply peaked about R_{top} given the large value of n, a feature which provides some justification for the deterministic treatment of nucleation. The constant c_n is determined from the constraint that $\langle R_{\text{isl}}\rangle = R_{\text{top}}$. Utilizing Eq. (A3), one obtains

$$(c_n)^{1/n} = n\int_0^\infty dy\, y^n \exp[-y^n], \qquad \text{(A4)}$$

so, e.g., $c_5 = 0.653$ and $c_6 = 0.637$ (where $n=6$ is used below). To implement stochastic nucleation, we determine a function $R_{\text{isl}} = R_{\text{isl}}(x)$ which recovers the correct distribution of island radii when x is selected as a uniformly distributed random number on $[0,1]$. It thus follows that $dx = p_{\text{nuc}}^*(R_{\text{isl}})dR_{\text{isl}}$, and consequently that

$$x = \int_0^{R_{\text{isl}}} p_{\text{nuc}}^*(R_{\text{isl}})dR_{\text{isl}} = 1 - P_{\text{nonuc}}. \qquad \text{(A5)}$$

In conclusion, one has that

$$R_{\text{isl}} = R_{\text{top}}\left[-\frac{\ln[1-x]}{c_n}\right]^{1/n}. \qquad \text{(A6)}$$

With this prescription, there is no upper limit on the range of R_{isl}. If R_{top}/R is significant, then some selected R_{isl} will likely exceed the mound radius, R. In this case, some refinement of the above probability distribution is required to impose an upper cuttoff of $R_{\text{isl}} < R$. However, in the analysis below, R_{top}/R is sufficiently small that effectively all selected R_{isl} are below R.

In our numerical analysis of the evolution of a finite mound with stochastic nucleation, we use Eq. (A6) to generate a sequence of values for R_{top} which are used for the nucleation of successive top layers. We integrate Eqs. (2), (3), and (4) for some time to let the system evolve into a steady state, then average mound profiles obtained over many ML of deposition. Figure 11 compares such mound

profiles for the deterministic and stochastic nucleation schemes. The profiles are similar except very near the mound peak, which is flat for deterministic nucleation but smooth (after averaging) for stochastic nucleation.

APPENDIX B: PERIODIC EVOLUTION OF A SEMI-INFINITE MOUND: $P_+ = 1$

Here, we determine the periodic solution for the evolution of a semi-infinite mound in the special case where $P_+ = 1$ and where the evolution equations adopt a simpler recursive form. Specifically, these equations become

$$\frac{dx_1}{d\theta} = -x_1 - c,$$

$$\frac{dx_n}{d\theta} = -(x_n - x_{n-1}), \quad \text{for } n > 1. \qquad \text{(B1)}$$

For the periodic solution just after the bottom step disappears, we assign the step positions as $x_n(\theta=0) = x_n^*$ for $n \geq 1$. Then, the above equations can be solved recursively with these initial conditions and the additional requirement of obtaining a periodic solution, i.e.,

$$x_1(\theta=1) = 0, \ x_2(\theta=1) = x_1^*, \ x_3(\theta=1) = x_2^*, \ldots. \qquad \text{(B2)}$$

Integrating these equations leads to the recursion relations

$$x_1^* = c(e-1), \qquad \text{(B3)}$$

$$x_2^* = (e-1)x_1^* - c(e-2), \qquad \text{(B4)}$$

$$x_n^* = (e-1)x_1^* - c(e-2) - \frac{1 + x_{n-2}^*}{2!} - \cdots$$

$$- \frac{1 + x_1^*}{(n-1)!}, \quad \text{for } n > 2. \qquad \text{(B5)}$$

It is convenient to recast these equations for the terrace widths, $L_0^* = x_1^*$, and $L_n^* = x_{n+1}^* - x_n^*$ for $n > 1$, as

$$L_0^* = c(e-1), \qquad \text{(B6)}$$

$$L_1^* = (e-1)L_0^* - c, \qquad \text{(B7)}$$

$$L_n^* = (e-1)L_{n-1}^* - \frac{L_{n-2}^*}{2!} - \cdots - \frac{L_1^*}{(n-1)!}$$

$$- \frac{ce}{n!}, \quad \text{for } n > 2. \qquad \text{(B8)}$$

Solving these equations yields

$$L_0^* = c(e-1) = 1.71828c, \qquad \text{(B9)}$$

$$L_1^* = c(e^2 - 2e) = 1.95249c, \qquad \text{(B10)}$$

$$L_2^* = c(e^3 - 3e^2 - 3e/2) = 1.99579c, \qquad \text{(B11)}$$

$$L_3^* = c(e^4 - 4e^3 + 4e^2 - 2e/3) = 2.00003c,\ldots \qquad \text{(B12)}$$

More direct analysis of the limiting behavior, as $n \to \infty$, which is of primary interest, comes from utilizing a suitable z transform $\hat{x}(z, \theta) = \sum_{n=1}^{\infty} z^n x_n(\theta)$. Applying this transform to the evolution equations yields a simple ordinary differential equation for $\hat{x}(z, \theta)$ which can be solved to obtain

$$\hat{x}(z, \theta) = \hat{x}(z, 0) e^{-(1-z)\theta} - \frac{z}{1-z}[1 - e^{-(1-z)\theta}], \quad \text{for } 0 < \theta < 1.$$
(B13)

Imposition of the boundary condition for a periodic solution requires that

$$\hat{x}(z, 1) = z\hat{x}(z, 0).$$
(B14)

Substituting into Eq. (B13) finally yields the result

$$\hat{x}(z, 0) = -\frac{z}{1 - z} \frac{\exp[1 - z] - 1}{z \exp[1 - z] - 1} \sim \frac{2c}{(1-z)^2}, \quad \text{as } z \to 1.$$
(B15)

Since $x_n^* \sim \text{const} + nL_\infty$ for large n, it follows that $\hat{x}(z, 0) \sim L_\infty/(1-z)^2$ as $z \to 1$, so $L_\infty = 2c$. In conclusion, we obtain the exact result $m_s^\infty = b/(2c)$ for $P_+ = 1$.

Finally, we note that for $P_+ < 1$, a recursive analysis is not possible. However, application of a suitable modified transform to the evolution equations should allow an exact treatment.

APPENDIX C: EXACT ANALYSIS OF A THREE-LEVEL SYSTEM

To further elucidate the periodic evolution of finite mounds (either with or without DF), it is natural to consider the "extreme" case corresponding to large $R_{\text{top}} < R$ where there are at most two steps. In this case, there are at most three levels of terraces, so the evolution corresponds to a so-called three-level system. Below, we set $R_{\text{top}} = R - x_c$, and assume constant $P_\pm$.

We consider an "initial" configuration for periodic evolution as corresponding to the time just after nucleation of the second upper island of step. See Fig. 12(a). Then, one has that $x_1(\theta=0) = x_c$, and $x_2(\theta=0) = R$.

There are two distinct stages of the mound evolution. In the first stage for $0 < \theta < \theta^*(<1)$, say, before x_1 reaches zero (at $\theta = \theta^*$), the mound has two steps as shown in Fig. 12(b). The evolution of these two steps is described by

$$\frac{dx_1}{d\theta} = -x_1 - P_-(x_2 - x_1) - c,$$
(C1)

$$\frac{dx_2}{d\theta} = -P_+(x_2 - x_1 - c) - (1 - x_2).$$
(C2)

It is more convenient to transform these equations introducing new dependent variables $x_2 - x_1$ and $x_2 + x_1$, noting that $d(x_2 + x_1)/d\theta = -R$. (There is a natural generalization of this latter relation for mounds with any number of steps.) Integrating these equations for $\theta < \theta^*$, one obtains

$$x_2 + x_1 = x_c + (1 - \theta)R,$$
(C3)
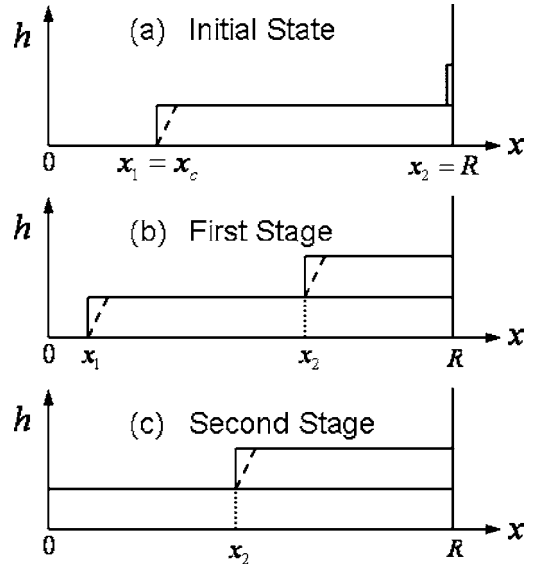
FIG. 12. Schematic of the evolution of a mound with at most two steps: (a) initial state, (b) first stage before x_1 reaches zero, (c) second stage where there is only one step following the disappearance of the original bottom step.

$$x_2 - x_1 = \left(\frac{x_c}{\Delta} + \frac{R}{\Delta^2} + c\frac{1+\Delta}{\Delta}\right)(1 - e^{-\Delta\theta}) + (R - x_c)e^{-\Delta\theta} - \frac{\theta R}{\Delta}.$$
(C4)

At $\theta = \theta^*$ when x_1 vanishes, these two quantities become equal, which imposes a key constraint on θ^* utilized below.

Finally, we note that in this first stage, the net step attachment flux is given by

$$K_{\text{tot}}^1/F = x_1 + x_2 - 1 + \Delta(x_2 - x_1 - c) - c$$
(C5)

and can thus be calculated exactly from the above results. Figure 12(c) illustrates the second stage of mound evolution where there is only one step, starting when x_1 vanishes at $\theta = \theta^*$ and ending when $x_2 = x_c$ at $\theta = 1$. In this regime, the evolution of step 2 is trivially given by
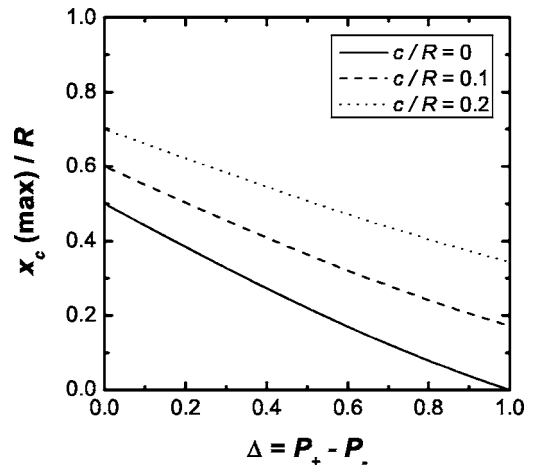
FIG. 13. The behavior of $x_c(\text{max})$ with Δ in the three-level system for the different choices of c/R.

$$\frac{dx_2}{d\theta} = -R, \tag{C6}$$

so $x_2 = x_c + (1-\theta)R$. The net step attachment flux in the second stage is given by

$$K_{\text{tot}}^2/F = 2x_2 - R, \tag{C7}$$

and can thus be readily calculated using Eq. (C6).

Next, we investigate the average value $\langle K_{\text{tot}} \rangle$, of K_{tot} over a period of 1 ML,

$$
\begin{aligned}
\left\langle \frac{K_{\text{tot}}}{F} \right\rangle &= \int_0^{\theta^*} d\theta K_{\text{tot}}^1/F + \int_{\theta^*}^1 d\theta K_{\text{tot}}^2/F \\
&= -\left(\frac{x_c}{\Delta} + \frac{R}{\Delta^2} + \frac{2c(1+\Delta)}{\Delta} \right)(1 - e^{-\Delta\theta^*}) \\
&\quad - (R - x_c)e^{-\Delta\theta^*} + \frac{\theta^* R}{\Delta} + 2x_c - \theta^* R. \tag{C8}
\end{aligned}
$$

Given the constraint on θ^* mentioned above, it follows that $\langle K_{\text{tot}} \rangle = 0$. This result holds for the general c (including $c=0$ corresponding to no DF).

Finally, we have noted that the above three-level system picture of periodic evolution applies only for sufficiently large R_{top} (or sufficiently small x_c). The specific condition for the maximum possible value $x_c(\max)$ of x_c comes from the constraint on θ^* mentioned above, after setting $\theta^* = 1$. Specifically, one obtains

$$x_c(\max) = \frac{\left(\frac{R}{\Delta^2} + c\frac{1+\Delta}{\Delta} \right)(1 - e^{-\Delta}) + Re^{-\Delta} - \frac{R}{\Delta}}{1 - \frac{1-e^{-\Delta}}{\Delta} + e^{-\Delta}}. \tag{C9}$$

For $\Delta = 0$, one has $x_c(\max) = R/2 + c$. For $\Delta = 1$, one has $x_c(\max) = c(e-1)$. The behavior of $x_c(\max)$ for the general case is shown in Fig. 13.

[1] T. Michely and J. Krug, *Islands, Mounds and Atoms: Patterns and Processes in Crystal Growth Far from Equilibrium* (Springer, Berlin, 2004).

[2] J. W. Evans, P. A. Thiel, and M. C. Bartelt, Surf. Sci. Rep. (to be published, 2006).

[3] G. Ehrlich and F. G. Hudda, J. Chem. Phys. **44**, 1039 (1966).

[4] R. L. Schwoebel and E. J. Shipsey, J. Appl. Phys. **37**, 3682 (1966).

[5] J. Villain, J. Phys. I **1**, 19 (1991).

[6] A. Pimpinelli and J. Villain, *Physics of Crystal Growth* (Cambridge University Press, Cambridge, 1998).

[7] H.-J. Ernst, F. Fabre, R. Folkerts, and J. Lapujoulade, Phys. Rev. Lett. **72**, 112 (1994).

[8] J. A. Stroscio, D. T. Pierce, M. D. Stiles, A. Zangwill, and L. M. Sander, Phys. Rev. Lett. **75**, 4246 (1995).

[9] J.-K. Zuo and J. F. Wendelken, Phys. Rev. Lett. **78**, 2791 (1997).

[10] C. R. Stoldt, K. J. Caspersen, M. C. Bartelt, C. J. Jenks, J. W. Evans, and P. A. Thiel, Phys. Rev. Lett. **85**, 800 (2000).

[11] K. J. Caspersen, A. R. Layson, C. R. Stoldt, V. Fournee, P. A. Thiel, and J. W. Evans, Phys. Rev. B **65**, 193407 (2002).

[12] M. Siegert and M. Plischke, Phys. Rev. Lett. **73**, 1517 (1994).

[13] M. C. Bartelt and J. W. Evans, Phys. Rev. Lett. **75**, 4250 (1995).

[14] P. Smilauer and D. D. Vvedensky, Phys. Rev. B **52**, 14263 (1995).

[15] J. G. Amar and F. Family, Phys. Rev. B **54**, 14742 (1996).

[16] J. W. Evans, D. E. Sanders, P. A. Thiel, and A. E. DePristo, Phys. Rev. B **41**, 5410 (1990).

[17] J. W. Evans, Phys. Rev. B **43**, 3897 (1991).

[18] H. C. Kang and J. W. Evans, Surf. Sci. **271**, 321 (1992).

[19] D. E. Sanders and J. W. Evans, in *The Structure of Surfaces III*, edited by S. Y. Tong, M. A. Van Hove, K. Takayanagi, and X. D. Xie (Springer, Berlin, 1991), pp. 38.

[20] D. E. Sanders, D. M. Halstead, and A. E. DePristo, J. Vac. Sci. Technol. A **10**, 1986 (1992).

[21] J. Yu and J. G. Amar, Phys. Rev. Lett. **89**, 286103 (2002).

[22] J. Yu and J. G. Amar, Phys. Rev. B **69**, 045426 (2004).

[23] M. Siegert and M. Plischke, Phys. Rev. E **53**, 307 (1996).

[24] J. G. Amar, Phys. Rev. B **60**, R11317 (1999).

[25] H.-C Jeong and E. D. Williams, Surf. Sci. Rep. **34**, 171 (1999).

[26] W. K. Burton, N. Cabrera, and F. Frank, Philos. Trans. R. Soc. London **243**, 299 (1951).

[27] N. Israeli and D. Kandel, Phys. Rev. Lett. **80**, 3300 (1998); Phys. Rev. B **60**, 5946 (1999); **62**, 13707 (2000).

[28] D. Margetis, M. J. Aziz, and H. A. Stone, Phys. Rev. B **69**, 041404 (2004); **71**, 165432 (2005).

[29] I. Elkinani and J. Villain, J. Phys. I **4**, 949 (1994).

[30] P. Politi and J. Villain, Phys. Rev. B **54**, 5114 (1996).

[31] J. Krug, J. Stat. Phys. **87**, 505 (1997).

[32] J. Krug, Physica A **313**, 47 (2002).

[33] W. E and N. K. Yip, J. Stat. Phys. **104**, 221 (2001).

[34] R. V. Kohn, T. S. Lo, and N. K. Yip, in *Statistical Mechanical Modeling in Materials Science*, edited by M. C. Bartelt *et al.*, MRS Symposia Proceedings No. 701 (Materials Research Society, Warrendale, PA, 2002), p. T1.7.

[35] Maozhi Li and J. W. Evans, Phys. Rev. Lett. **95**, 256101 (2005); Phys. Rev. Lett. **96**, 079902(E) (2006).

[36] J. Tersoff, A. W. Denier van der Gon, and R. M. Tromp, Phys. Rev. Lett. **72**, 266 (1994).

[37] J. Rottler and P. Maass, Phys. Rev. Lett. **83**, 3490 (1999).

[38] J. Krug, P. Politi, and T. Michely, Phys. Rev. B **61**, 14037 (2000).

[39] C. Castellano and P. Politi, Phys. Rev. Lett. **87**, 056102 (2001).

[40] Note that another viable implementation of top layer nucleation would set $x_{n^*+1} = R - c$ so $L_{n^*} = c$ at the time of nucleation, $t = t'_{n^*+1}$. Behavior will not vary significantly from that for the choice $x_{n^*+1} = R$ so $L_{n^*} = 0$ used in this study. Note that the last two terms in Eq. (4) can be contracted as $-FL_{n^*}$, which varies smoothly in either case.

[41] The three-step approximation yielded ill-behaved (complex-valued) solutions, and thus cannot be used.

[42] P. Politi, cond-mat/0601655, C. R. Phys. (to be published).

[43] M. Siegert, Phys. Rev. Lett. **81**, 5481 (1998).

[44] L. Golubovic, A. Levandovsky, and D. Moldovan, Phys. Rev.

Lett. **89**, 266104 (2002).

[45] A. Levandovsky and L. Golubovic, Phys. Rev. B **69**, R241402 (2004).

[46] R. V. Kohn and X. Yan, Commun. Pure Appl. Math. **56**, 1549 (2003).

[47] B. Li and J.-G. Liu, Eur. J. Appl. Math. **14**, 713 (2003).

[48] P. Politi, G. Grenet, A. Marty, A. Ponchet, and J. Villain, Phys. Rep. **324**, 271 (2000).

[49] J. G. Amar and F. Family, Phys. Rev. B **54**, 14 071 (1996).

[50] J. G. Amar and F. Family, Phys. Rev. Lett. **77**, 4584 (1996).

[51] V. Borovikov and J. G. Amar, Phys. Rev. B **72**, 085460 (2005).

[52] M. C. Bartelt and J. W. Evans, in *Evolution of Epitaxial Structure and Morphology*, edited by Andrew Zangwill *et al.*, MRS Symposia Proceedings No. 399 (Materials Research Society, Warrendale, PA, 1996), p. 89.

[53] M. C. Bartelt and J. W. Evans, Surf. Sci. **423**, 189 (1999).

[54] In $(2+1)$D, one obtains $n=7$ for $L_{ES} \gg L_{isl}$, and $n=8$ for $L_{ES} \ll L_{isl}$.